BNL-225984-2024-JAAM

Investigation of defect formation at the early stage of PVT-grown 4H-SiC crystals

S. Hu, X. Tong

To be published in "Journal of Crystal Growth"

February 2024

Center for Functional Nanomaterials
Brookhaven National Laboratory

U.S. Department of Energy
USDOE Office of Science (SC), Basic Energy Sciences (BES). Scientific User Facilities (SUF)

DISCLAIMER

Investigation of Defect Formation at the Early Stage of PVT-grown 4H-SiC Crystals

Shanshan Hu [a], Yafei Liu [a], Qianyu Cheng [a], Zeyu Chen [a], Xiao Tong [b], Balaji Raghothamachar [a], Michael Dudley [a]
[a] Department of Materials Science & Chemical Engineering, Stony Brook University, Stony Brook, NY 11794 USA
[b] Center for Functional Nanomaterials, Brookhaven National Laboratory, Upton, NY 11973, USA

Shanshan Hu (shanshan.hu@stonybrook.edu), Yafei Liu (yafei.liu@stonybrook.edu), Qianyu Cheng (qianyu.cheng@stonybrook.edu), Zeyu Chen (zeyu.chen@stonybrook.edu), Xiao Tong (xtong@bnl.gov), Balaji Raghothamachar (balaji.raghothamachar@stonybrook.edu), Michael Dudley (michael.dudley@stonybrook.edu)

Abstract

Several 4° off-axis 4H-SiC wafers with several hundred microns of initial-stage growth by PVT method are investigated by Synchrotron Monochromatic Beam X-ray Topography (SMBXT). Defect behavior across the seed/newly grown layer interface are demonstrated. Comparison of early stage grown layers to seed sample indicates generation of threading edge dislocation (TED) and threading screw dislocation (TSD)/ threading mixed dislocation (TMD) pairs at the interface while most basal plane dislocations (BPDs) are deflected into TEDs. The (0001) facet of the crystal is already formed at early stage growth at the edge of the wafer and high nitrogen incorporation in facet leads to conditions favorable for nucleation and glide of Shockley/double Shockley faults with layers of 3C-SiC deposited on facet acting as nuclei. Unique-shaped dislocations are observed at early stage growth, which are caused by deflection of TSDs/TMDs and TEDs by macrosteps near the periphery of the sample and the subsequent glide of the **a** components. The effect of the quality of the seed surface before growth is manifested as randomly oriented arrays of pairs of TEDs and TSDs/TMDs on the as grown surface resulting from residual surface damage from scratches.

Introduction

Silicon Carbide, typically 4H-SiC, due to its excellent electrical and thermal properties, has been replacing conventional silicon materials, which are considered to have reach their limit, for high power and high frequency applications[1]. The demand for high quality SiC wafers with low defect density is rapidly increasing especially for automotive and energy saving applications. Over the past few decades, various types of defects existing in 4H-SiC substrate crystal have demonstrated their detrimental effects to the reliability of the subsequent power devices[2]. Therefore, it is important to understand the formation mechanism and the behavior of various defects during crystal growth of 4H-SiC wafers. Some significant observations include the replication of threading dislocations from the seed through the grown crystal as well as dislocation pair nucleation at the seed/newly grown layer interface [3]; deflection of TSDs/TMDs with Burgers vector of **c** and **c**+**a** by the overgrowth of macrosteps leading to stacking fault formation on the basal plane[4]; and Shockley stacking faults generated from residual surface scratches in region of higher doping concentration after the wafers subjected to heat treatment.[5].

Numerous efforts have been expended to optimize growth process to lower defect density of SiC wafers obtained from bulk growth by physical vapor transport (PVT) method[6]. One major approach is the study of early stages of crystal growth as most defects are nucleated at this stage and propagate into the boule. Nucleation of threading edge dislocations (TEDs) and threading screw dislocations (TSDs) at the early growth stage in PVT-grown SiC is revealed by Sanchez et al[7]. Behaviors of TEDs, TSDs/threading mixed dislocations (TMDs), and basal plane dislocations (BPDs) across the seed/newly grown layer interface in PVT-grown 4H SiC are demonstrated by Ailihumaer et al.[8]. Recently, we have reported on the multiple types of stacking fault formation in the off-facet region at early-stage growth of 4H-SiC crystals[9].

However, additional detailed investigations are necessary during early stage of growth for continued understanding and optimization for PVT growth of 4H-SiC crystals. In this study, several 4° off-axis 4H-SiC wafers with several hundred microns of early-stage growth are prepared by PVT method. Synchrotron X-ray topography (SXRT) complemented by Nomarski optical microscopy (NOM) are employed to evaluate defect characteristics during early stage growth, which provide more insights on defect formation and multiplication forming the basis for the subsequent growth of the full crystal boule.

Experimental

Two 6 inch 4° off-axis (0001) PVT-grown SiC wafers, which have newly grown layer with thickness of several hundred microns grown on the C-face of the seed under low C/Si conditions, were prepared. A reference seed wafer cut from the same boule as the seed of one of the early grown wafer was used to represent the defect distribution in the seed. Samples were imaged by Synchrotron Monochromatic X-ray Topography (SMBXT) in grazing incidence geometry at beamline 1-BM, Advanced Photon Source at Argonne National Laboratory. In grazing geometry, the incident angle is set at ~2.1°, specimen-film distance at 40cm, and X-ray topographic images were recorded on the Agfa Structurix D3-SC films with resolution of ~1um. For detailed defect characterization, $11\bar{2}8$, $\bar{1}2\bar{1}8$, $2\bar{1}\bar{1}8$, $2\bar{2}0\ 10$ reflections were recorded. TSDs, TEDs and BPDs are all visible in $11\bar{2}8$, $\bar{1}2\bar{1}8$, $2\bar{1}\bar{1}8$ reflections based on the g·b criteria while stacking fault contrast shows up in $2\bar{2}0\ 10$ reflection according to g·R criteria[10]. Macroscopic morphology of the newly grown surface was examined by Nomarski differential interference contrast (DIC) optical microscopy. Raman spectroscopy at selected points and 2D Raman mapping were carried out using the WITec Confocal Raman Microscope Alpha 300 to check the polytypes across the wafers. For Burgers vector characterization of dislocations, individual dislocation images on X-ray topographs are compared with images simulated by ray tracing simulation method[11, 12], which is conducted by Python3 software on personal computer.

Results and Discussion

<u>Dislocation behavior across the seed/newly grown layer interface</u>

To investigate dislocation behavior across the seed/newly grown layer interface, statistical analysis is applied for 9 regions across the wafer as shown in Figure 1(a) for both reference seed wafer and newly grown layer. Since reference seed wafer is cut from the same boule as the seed of the newly grown layers, the defect distribution of reference seed wafer is similar to that in the seed of the newly grown layer. From the result for TEDs as shown in Figure 1(b), significant increase in TED densities for all the 9 regions throughout the wafer from the reference seed wafer to newly grown layer is observed. TED pairs, which could nucleate at seed/newly grown layer interface, are observed by X-ray topograph for the newly grown layer as shown in Figure 1(e). Thus, in addition to the replication of TEDs from the seed, nucleation of TED pairs at the seed/newly grown layer interface also contributes to the density of TEDs for the newly grown layer. Another source for the TED density for the newly grown layer is redirection of BPDs in the seed since BPDs density significantly decreased in the newly grown layer compared to the seed as shown by Figure 1(c). Most BPDs in the seed are redirected into threading direction at the seed/newly grown layer interface. Similar with TEDs, TSDs/TMDs densities undergo significant increases also for the newly grown layer especially at the positions away from the center for the sample, such as region 1 and 2. The reason for the increased density of TSDs/TMDs for such regions could relate to the lattice mismatch arising from thermal stress and/or the nitrogen concentration difference between the seed and grown crystals from higher temperatures since the positions away from the center are closer to the heating source during growth.[13] X-ray topograph shows multiple TSD/TMD pairs in the regions away from center of the sample as shown by Figure 1(e). Replication of TSDs/TMDs from the seed and TSD/TMD pair nucleation at the seed/newly grown layer interface are two contributors for the density of TSDs/TMDs in newly grown layer.

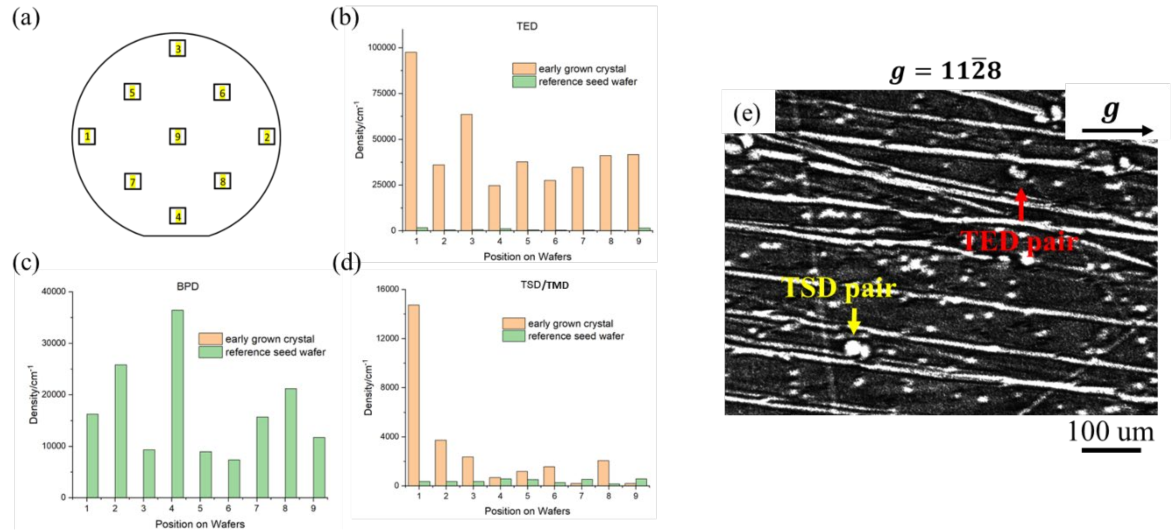

Figure 1. Statistical analysis is applied for 9 regions across the wafer as shown in (a) for both reference seed wafer and early grown layer. The results for TEDs, BPDs, and TSDs/TMDs are shown by (b), (c), (d), respectively. Orange boxes represent the statistically analyzed result for early grown crystal while the green boxes show the result for reference seed wafer. TED and TSD/TMD pairs, which are observed by SMBXT images with $11\bar{2}8$ reflection as shown by (e), contribute to the TEDs and TSDs/TMDs density in early grown crystal.

To further confirm the dislocation behavior across the seed/newly grown layer interface obtained by statistical analysis, the $11\bar{2}8$ SMBXT images of one 4H-SiC early grown crystal from the exact same region for the back side (seed crystal) and the front side (early grown layer) were compared. Comparing the two topographic images, most of the TSDs/TMDs as marked in yellow circles show up in both images, indicating they are replicated from the seed to the newly grown layer. Some TSDs/TMDs marked in blue circles only show up in the crystal seed but are not visible in the newly grown layer, suggesting that these dislocations may have been deflected onto the basal plane and become Frank dislocations by overgrowth of macro-steps. On the other hand, there are some TSDs/TMDs marked in red circles shown in newly grown layer and not visible in the seed, which suggest that these dislocations are nucleated in opposite sign pairs at the seed/newly grown layer interface. BPDs are observed in the seed but not after growth, indicating BPDs are redirected into TEDs at the seed/newly grown layer interface.

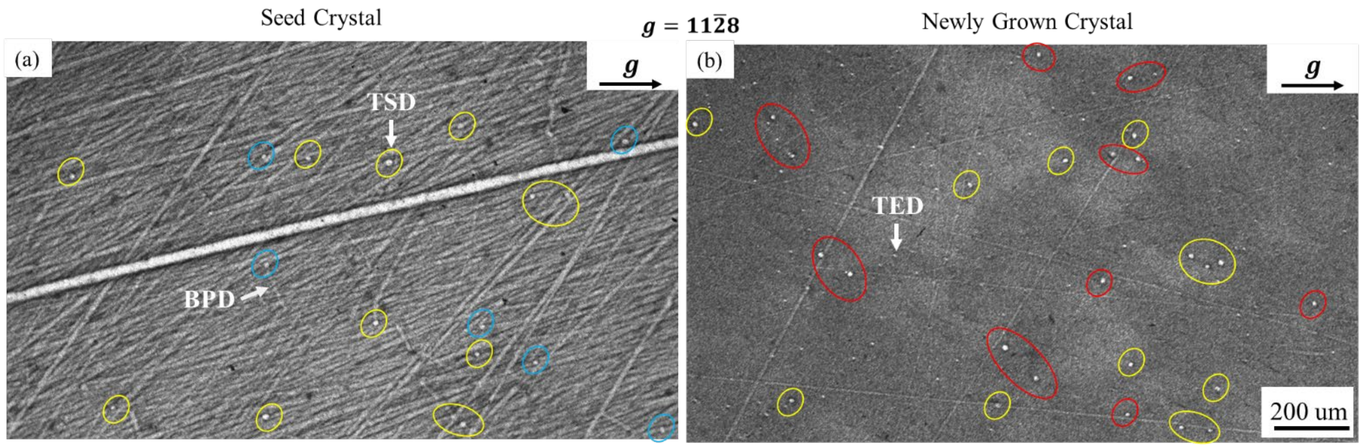

Figure 2. SMBXT images recorded in $11\bar{2}8$ reflection showing dislocation behavior in (a) the seed crystal and (b) the newly grown crystal. TSDs/TMDs marked in yellow circles are replicated into the grown crystal. TSDs/TMDs marked in blue circles get deflected onto basal plane by the step flow of macro-steps. TSDs/TMDs marked in red circles are newly generated at the seed/crystal interface.

Stacking fault formation in the facet

Facet formation is critical for the PVT grown 4H-SiC crystals since growth steps emanate from the facet and propagate to the remaining parts of the crystal. At the early stage growth, the facet is observed to already be formed at the edge of the wafer at the position shown by Figure 3(a). X-ray topographs from the facet region reveal distinct straight dislocation segments along <$11\bar{2}0$> directions with black or white contrast forming rhombus shapes as shown in Figure 3(b). The region bounded by dislocations shows area contrast in $2\bar{2}0$ 10 reflection as shown in Figure 3(c). Based on g·R analysis, Shockley stacking fault with fault vector of 1/3<$1\bar{1}00$> has area contrast in $2\bar{2}0$ 10 reflection[14]. Thus, Shockley stacking fault is formed on the facet and dislocations bounding stacking fault region are likely Shockley partial dislocations.

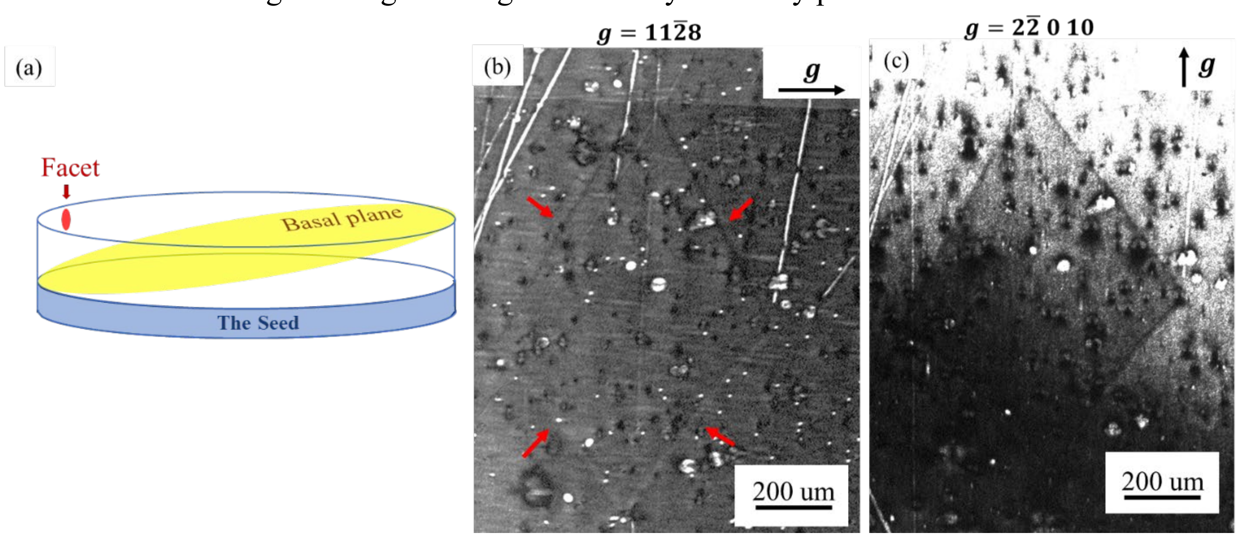

Figure 3. (a) The position of the facet relative to the basal plane at the early stage growth, and the SMBXT images recorded inside the facet in (b) $11\bar{2}8$ and (c) $2\bar{2}0\ 10$ reflections, showing dislocation segments lying along <$11\bar{2}0$> directions bounding a rhombus shaped region, that shows area contrast in $2\bar{2}0\ 10$ reflection indicating the presence of a stacking fault. The dislocation segments lying along <$11\bar{2}0$> directions are marked by red arrows in (b).

Ray tracing simulation of different 1/3<$1\bar{1}00$> partial dislocations along the <$11\bar{2}0$> directions were carried out to further identify the fault vectors for these Shockley stacking faults. For the rhombus loop of partial dislocations indicated by red arrows in Figure 3(b), it is found that when the Burgers vector is 1/3[$\bar{1}100$], the simulated images for the partial dislocations along each side as shown in Figure 4(a) match the contrast on topographic image. The deformed rhombus drawn by black line in Figure 4(a) reproduces the shape of partial dislocations on the topograph in Figure 3(b), indicating the simulated images of partial dislocations correlate with the images of partial dislocations forming the rhombus shape on the topograph. Figure 4(b) and 4(c) show the comparison of the contrast of partial dislocation along [$2\bar{1}\bar{1}0$] direction on topograph and its ray tracing simulated image. The width of the partial dislocation on the topograph is ~15 um, comparable to its width in the simulated image, which is ~13 um. On the other hand, on both the topograph and simulated image, the top two partial dislocations have black contrast while the bottom two partial dislocations have white contrast. From this, the fault vector for the rhombus shaped stacking fault region bounded partial dislocations is identified as 1/3[$\bar{1}100$].

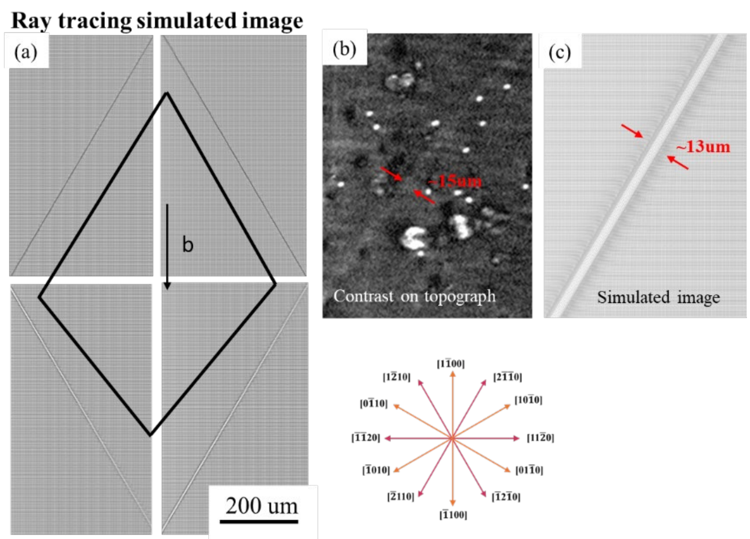

Figure 4. (a) Ray tracing simulated images for partial dislocations in Figure 3(b) marked by red arrows. The configuration of partial dislocations on topograph in Figure 3(b) is represented by the black deformed rhombus. The simulated images of partial dislocations correlate with the images of partial dislocations forming the rhombus shape on the topograph. The high magnification comparison for the partial dislocation along [$2\bar{1}\bar{1}0$] direction between (b) the contrast on topograph and (c) simulated image shows consistency with similar width and the same black/white contrast.

Similar rhombus shaped Shockley stacking fault formation have been observed by Yang et al.[5]. They reported the observation of overlapping Shockley stacking faults generated from residual surface scratches in regions of higher doping concentration after the wafers have been subjected to heat treatment. Note that as shown in Figure 5(a), the signs of partial dislocations can be identified by the distinct contrast features generated by the opposite signs of the edge Burgers vector component in grazing geometry SMBXT images. By comparing the observed image with the result predicted by the ray tracing simulation, the partial core structure can be determined. As a result, on the C-face of the early grown crystal, the C core partial dislocations have white contrast and the Si core partial dislocations have black contrast. Therefore, as shown in Figure 5(b), the C core partial dislocations are located at the top of the rhombus shaped loop, which is closer to the nucleation site at the top corner, while the Si core partial dislocations are at the bottom of the rhombus shape. The Si core partial dislocations glide since they have higher mobility than the C core partial dislocations and cause the expansion of stacking fault. The mechanism of stacking fault expansion is schematically shown in shown in Figure 5(c): At high temperatures during crystal growth, the hexagonal shaped partial dislocation loops nucleated have each of the segments initially lying in the low-energy Peierls valley, i.e. along <$11\bar{2}0$> directions. In addition, the partial segments have a Burgers vector of 1/3<$1\bar{1}00$>. Each partial segment comprising the hexagonal loop is either 30° or 90° character with cores comprising either Si or C atoms. The Si core partial is mobile, whereas the C core partial is sessile, so that both 30° and 90° Si partials glide while the C core partials are stationary but the segments are elongated due to the glide of Si core partials. Additionally, the 90° character Si core partials move faster than the 30° Si core partials, so that the 90° Si core partials eventually move out, leaving behind the 30° Si partials. Thus, the final configuration is a rhombus shaped stacking fault bounded by 30° Si and C core partials. Across the facet, several Shockley faults of different Burgers vectors are observed following the same nucleation and expansion mechanism but resulting in more complex shapes.

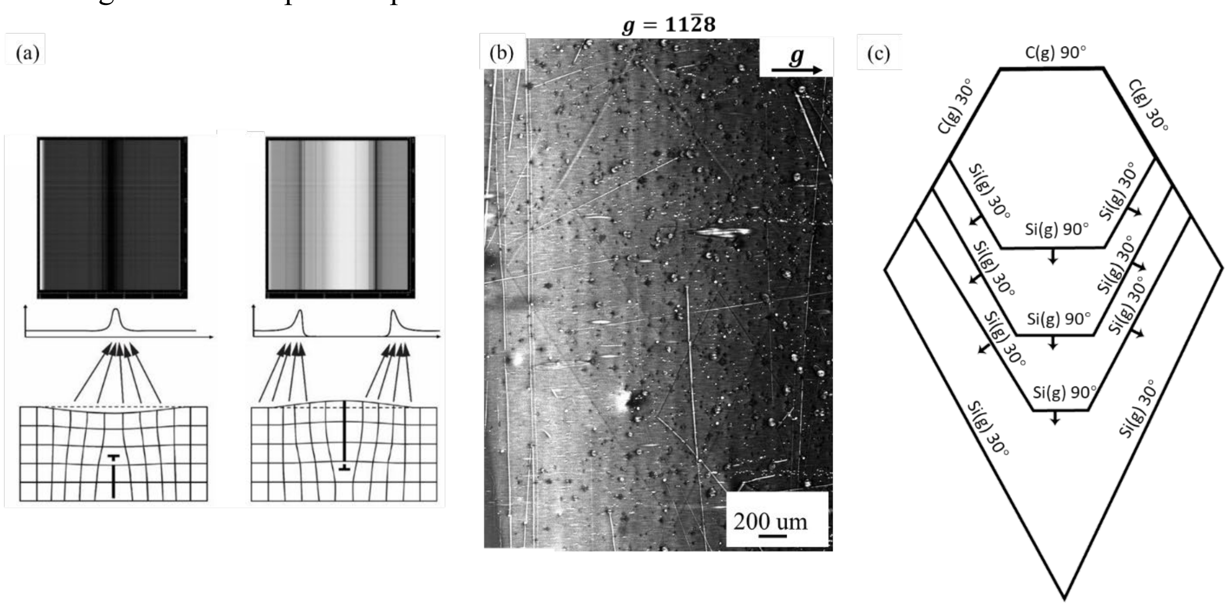

Figure 5. (a) In grazing geometry SMBXT images, the partial dislocation exhibits black contrast (i.e. the core causes convergence in the locally diffracted rays) if it extends away from that surface, and white contrast (i.e. the core causes divergence in the locally diffracted rays) if the extra half-plane extends toward the imaged surface[15]. (b) SMBXT image for rhombus shaped partial dislocation loops with $11\bar{2}8$ reflection showing the C core partial dislocations with white contrast are closer to the nucleation site at the top corner of the loops while the Si core partial

dislocations with black contrast glide away from the nucleation site and cause the expansion of the stacking fault region. (c) Schematic showing the rhombus shaped stacking fault configuration generated from a hexagonal partial loop with Burgers vector of 1/3<$1\bar{1}00$> and side along <$11\bar{2}0$> Peierls valleys. The 90° Si core partial eventually moves out after this process.

Two factors are considered to account for the formation of Shockley/double Shockley stacking faults on the facet during 4H-SiC PVT growth. Firstly, this SiC crystal was grown under low C/Si ratio conditions resulting in high nitrogen incorporation especially at the facet, which favor the expansion of Shockley/double Shockley stacking faults[16]. Secondly, some of the growth hillocks on the facet contain layers of 3C polytype embedded that can act as nucleation sites for the Shockley/double Shockley stacking faults[17]. In fact, when the nitrogen doping concentration exceeds a certain threshold, which is around 2-5x10^{19}cm^{-3}, the 3C nuclei likely undergoes stacking fault expansion. The nitrogen concentration for PVT grown 4H-SiC inside the facet region is much higher than that of off facet region and reaches magnitude of 10^{19}cm^{-3}[18]. The facet region of our sample could have nitrogen concentration with magnitude of 10^{19}cm^{-3} which favors the stacking fault expansion from 3C nuclei in the facet.
Thus, the growth hillocks in the facet, which are observed at the nucleation site of the Shockley/double Shockley stacking fault inside the facets, are examined by Raman spectroscopy. As shown by Figure 6(a), increased intensity of FTO(0) mode at 796cm^{-1} is observed for multiple hillocks, suggesting the existence of 3C structure. DIC optical image for one of the hillocks is shown in Figure 6(b). Spatial map of Raman intensity from the FTO(0) mode at $796cm^{-1}$ is applied for the region marked by red dashed square. As shown in Figure 6(c), the spatial map of Raman exhibits nonuniform distribution for the intensity at $796cm^{-1}$. The brighter region with higher intensity is where the 3C-SiC is located at, implying 3C-SiC layers could be deposited on the facet by 2D nucleation.

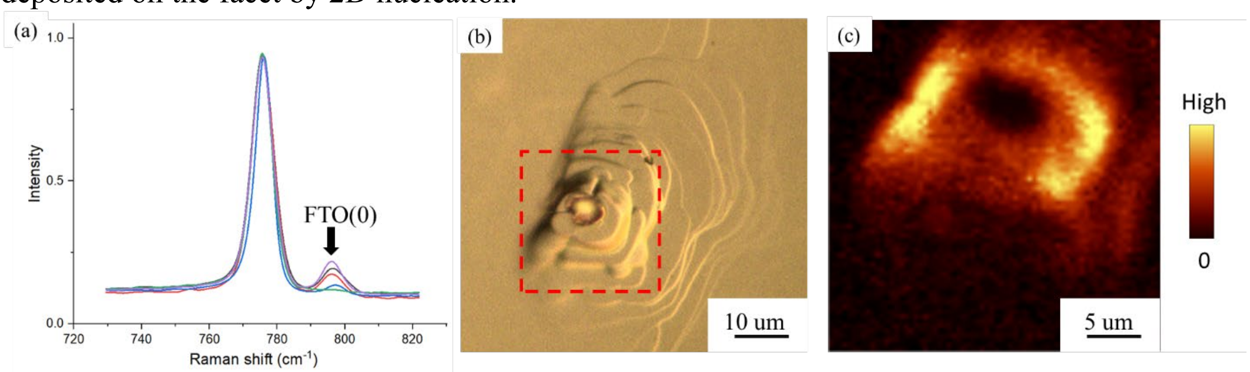

Figure 6. (a) Raman spectroscopy results for five hillocks in the facet. Different colored lines represent results from different hillocks. Increased intensity for FTO(0) mode is observed for 4 of five hillocks, which have blue, red, black, and purple color, suggesting existence of 3C structure. 3C structure is further confirmed by applying spatial map of Raman intensity for the region marked by red dashed square in (b) DIC image for one of the hillocks. (c)The result shows 3C distribution at the brighter region with higher intensity.

Deflection of TED and TMD pairs

The periphery of the newly grown crystal is characterized by significant deflection of TEDs and TSDs/TMDs which are caused by macrosteps as well as dislocations with unique configurations.

One type of unique shaped dislocation is shown by Figure 7(a). The dislocation is composed of two segments – upper one straight and the lower one curved indicating glide. By measuring the topographic image width of this dislocation (13~15um) and comparing it with the result from ray tracing simulated images for edge and mixed type dislocations, we found out that these dislocations have similar widths to edge type dislocations. Ailihumaer et al.[8] observed dislocations with similar unique shape and width at early stage 4H-SiC growth. They observed dislocations have Y-shaped feature and propose that the unique Y-shape is possibly formed by deflection of two opposite sign TEDs pair with Burgers vector of +**a** and -**a** by overgrowth of macrosteps followed by gliding away of the two newly created BPD segments of opposite sign from each other under the influence of the same thermal stress. A similar mechanism is employed to illustrate the formation mechanism for dislocation in Figure 7(a) as shown by Figure 7(b): The opposite sign TED pair deflect onto basal plane by overgrowth of macrosteps and generate two BPD segments. Different from Ailihumaer et al.'s observation where two BPD segments glide away from each other under the same thermal stress, the two BPD segments formed in our sample are under different stress condition even though they are narrowly spaced. Consequently, only one BPD segment glides away while the other remains straight, forming the unique shape shown in Figure 7(a).
Another type of unique shaped dislocation is shown by Figure 7(c), which have a straight segment at the bottom marked as **c** and a curved segment at the top marked as **a**. The two dislocation segments from this type of unique shaped dislocation show significantly different characteristics, which could be due to deflection of TMDs with Burgers vector containing both **a** and **c** components. Such unique shaped dislocations are also observed by Ailihumaer et al.[8]. Based on their analysis, the formation mechanism for this type of unique shaped dislocation is illustrated by Figure 7(d), where **a** component glides, but the **c** component remains stationary after TMD is deflected onto the basal plane.

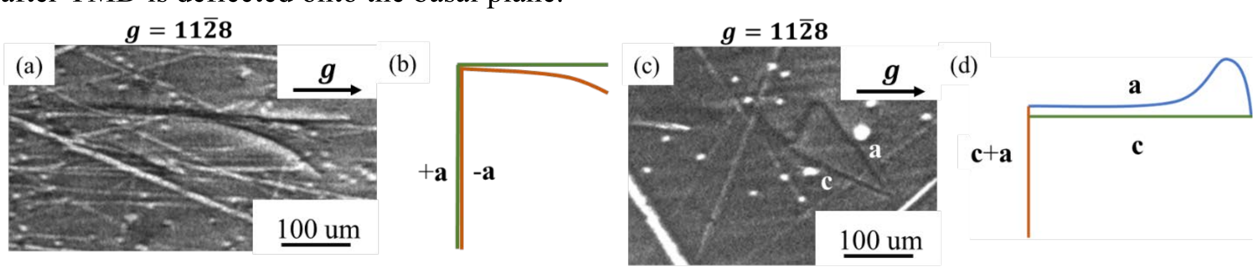

Figure 7. SMBXT images with $11\bar{2}8$ reflection for (a)(c) two types of dislocations with unique configurations. (b)(d) illustrate the formation mechanism for dislocations in (a)(c), respectively. The unique shape of dislocation in (a) is formed by deflection of an opposite sign TED pair followed by glide of one of the newly created BPD segments. The dislocation in (c) is formed by deflection of a TMD with **a** component glides and **c** component remains straight.

Seed surface preparation evaluation

Characterization of the newly grown layer of 4H-SiC crystal can offer information on the surface preparation of the seed wafer before growth. Figure 8(a) shows an example of a SMBXT image containing dislocation arrays marked by yellow arrows composed of TED pairs while the dislocation arrays marked by red arrows are formed by TSD/TMD pairs. Since the TED pair arrays and TSD/TMD pair arrays are oriented in random directions, they are likely nucleated at the surface damage from scratches on the seed surface at the very initial stage of crystal growth.

Zhang et al.[19] observed arrows of TED pairs in 4H-SiC epilayer associated with scratches on the substrate surface. Residual damage associated with scratches on the substrate surface is expected to have dislocation half-loops associated with them and their surface intersections act as sites from which dislocations propagate via replication during homo-epitaxial growth. The half-loops whose surface intersections are edge in character will propagate into the epilayer as TEDs and form arrays of TED pairs. The TED pair arrays observed in our sample can be explained by such formation mechanism also, which is illustrated by Figure 8(b). TSDs can nucleate at the scratch at the seed/newly grown layer interface also in form of pairs following similar formation mechanisms as shown by Figure 8(c).

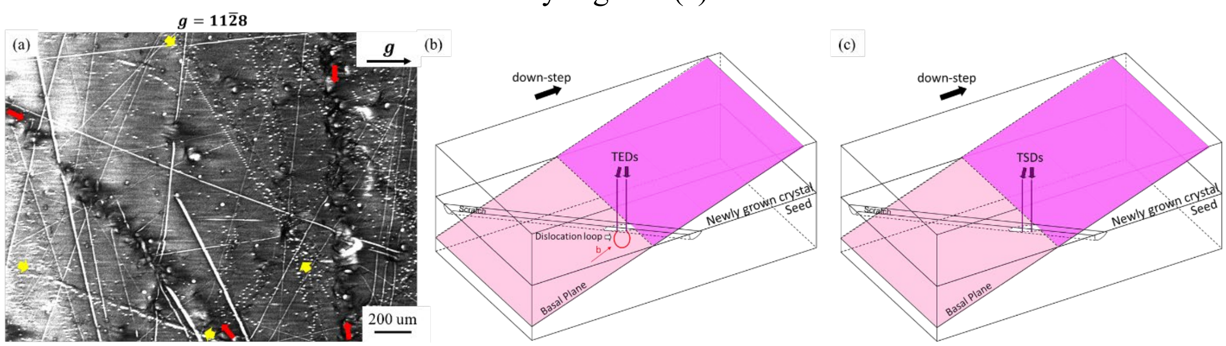

Figure 8. (a) SMBXT image for $11\bar{2}8$ reflection showing arrays of TED pairs (marked by yellow arrows) and TSD pairs (marked by red arrows) formed at the seed/newly grown layer interface at the scratches on the seed surface at the very initial stage of crystal growth and the accordingly schematics for formation mechanisms for (a) TED pairs and (b) TSD pairs at scratches on the seed surface. Note: Randomly oriented black/white lines on the image are contrast from scratches on the sample surface created from handling the wafer during seed side polishing.

Summary

Analysis of microstructure during early stage of PVT 4H-SiC growth is conducted by SWBXT, DIC optical microscopy, and the complementary Raman spectroscopy to enhance understanding of defect nucleation mechanisms. Comparison of early stage grown layers to seed sample indicates generation of TSD and TED pairs at the interface while most BPDs are deflected into TEDs. High nitrogen incorporation in facet leads to conditions favorable for nucleation and glide of Shockley/double Shockley stacking faults with layers of 3C-SiC deposited on facet acting as nuclei. Macrosteps cause significant deflection of TEDs and TSDs/TMDs near the periphery of the samples. The gliding of **a** component of dislocation after the deflection of TEDs and TSDs/TMDs results in unique shaped dislocations. The observation of randomly oriented arrays of TEDs and TSDs/TMDs pairs on the as grown surface of the newly grown layer indicate that surface preparation of seed wafer before growth to remove all damage is essential to reduce defect nucleation.

Acknowledgement

This work was supported by Pallidus, Inc.. Topography experiments were carried out at the Advanced Photon Source, a U.S. Department of Energy (DOE) Office of Science User Facility operated for the DOE Office of Science by Argonne National Laboratory. The Joint Photon Sciences Institute at SBU provided partial support for travel and subsistence for access to

Advanced Photon Source. This research used proximal probes of the Center for Functional Nanomaterials (CFN), which is a U.S. Department of Energy Office of Science User Facility, at Brookhaven National Laboratory under Contract No. DE-SC0012704. The ray tracing simulation work is supported by my colleague Hongyu Peng.

Reference

[1] H. Matsunami, T. Kimoto, Step-controlled epitaxial growth of SiC: High quality homoepitaxy, Mater. Sci. Eng. R Rep. 20 (1997) 125-166. https://doi.org/10.1016/S0927-796X(97)00005-3
[2] R. SIngh, M. PEchT, Commercial impact of silicon carbide, IEEE Ind. Electron. Mag. 2 (2008) 19-31. https://doi.org/10.1109/MIE.2008.928617.
[3] M. Dudley, S. Wang, W. Huang, C.H. Carter Jr, V. Tsvetkov, C. Fazi, White-beam synchrotron topographic studies of defects in 6H-SiC single crystals, J. Phys. D: Appl. Phys. 28 (1995) A63. https://doi.org/10.1088/0022-3727/28/4A/012
[4] M. Dudley, H.H. Wang, F.Z. Wu, S.Y. Byrapa, B. Raghothamachar, G. Choi, E. Sanchez, D.M. Hansen, R. Drachev, S.G. Mueller, Formation mechanism of stacking faults in PVT 4H-SiC created by deflection of threading dislocations with Burgers vector c+ a, Mater. Sci. Forum 679 (2011) 269-272. https://doi.org/10.4028/www.scientific.net/MSF.679-680.269
[5] Y. Yang, J. Guo, O. Goue, B. Raghothamachar, M. Dudley, G. Chung, E. Sanchez, J. Quast, I. Manning, D. Hansen, Effect of doping concentration variations in PVT-grown 4H-SiC wafers, J. Electron. Mater. 45 (2016) 2066-2070. https://doi.org/10.1007/s11664-016-4378-8
[6] I. Manning, Y. Matsuda, G. Chung, E. Sanchez, M. Dudley, T. Ailihumaer, B. Raghothamachar, Progress in bulk 4H SiC crystal growth for 150 mm wafer production, Mater. Sci. Forum 1004 (2020) 37-43. https://doi.org/10.4028/www.scientific.net/MSF.1004.37
[7] E. Sanchez, J. Liu, M. De Graef, M. Skowronski, W. Vetter, M. Dudley, Nucleation of threading dislocations in sublimation grown silicon carbide, J. Appl. Phys. 91 (2002) 1143-1148. https://doi.org/10.1063/1.1428088
[8] T. Ailihumaer, H. Peng, Y. Liu, B. Raghothamachar, M. Dudley, G. Chung, I. Manning, E. Sanchez, Synchrotron X-ray topography studies of dislocation behavior during early stages of PVT growth of 4H-SiC crystals, J. Electron. Mater. 50 (2021) 3258-3265. https://doi.org/10.1007/s11664-021-08827-6
[9] S. Hu, Y. Liu, Z. Chen, Q. Cheng, B. Raghothamathar, M. Dudley, D. Dukes, V. Torres, L. Young, S. Griswold, H. Bricetti, C. Liu, Y. Zhu, Analysis of defect structures during the early-stages of PVT growth of 4H-SiC crystals, Mater. Sci. Forum, submitted.
[10] A. Authier, Y. Epelboin, Variation of stacking fault contrast with the value of the phase shift in X-ray topography, Phys. Status Solidi A 41 (1977) K9-K12. https://doi.org/10.1002/pssa.2210410146
[11] M. Dudley, X. Huang, W. Huang, Assessment of orientation and extinction contrast contributions to the direct dislocation image, J. Phys. D: Appl. Phys. 32 (1999) A139. https://doi.org/10.1088/0022-3727/32/10A/329
[12] X. Huang, M. Dudley, W. Vetter, W. Huang, W. Si, C. Carter Jr, Superscrew dislocation contrast on synchrotron white-beam topographs: an accurate description of the direct dislocation image, J. Appl. Crystallogr. 32 (1999) 516-524. https://doi.org/10.1107/S0021889899002939

[13] H. Suo, S. Tsukimoto, K. Eto, H. Osawa, T. Kato, H. Okumura, Evaluation of the increase in threading dislocation during the initial stage of physical vapor transport growth of 4H-SiC, Jpn. J. Appl. Phys. 57 (2018) 065501. https://doi.org/10.7567/1347-4065/aae92e
[14] K. Konishi, R. Fujita, K. Kobayashi, A. Yoneyama, K. Ishiji, H. Okino, A. Shima, T. Ujihara, In-operando x-ray topography analysis of SiC metal–oxide–semiconductor field-effect transistors to visualize stacking fault expansion motions dynamically during operations, J. Appl. Phys. 130 (2021) 145703. https://doi.org/10.1063/5.0063082
[15] X. Huang, D.R. Black, A. Macrander, J. Maj, Y. Chen, M. Dudley, High-geometrical-resolution imaging of dislocations in SiC using monochromatic synchrotron topography, Appl. Phys. Lett. 91 (2007) 231903. https://doi.org/10.1063/1.2814032
[16] H.J. Chung, S.W. Huh, A. Polyakov, S. Nigam, Q. Li, J. Grim, M. Skowronski, E. Glaser, W. Carlos, J.A. Freitas, Electrical properties of undoped 6H-and 4H-SiC bulk crystals grown by halide chemical vapor deposition, Mater. Sci. Forum 527 (2006) 625-628. https://doi.org/10.4028/www.scientific.net/MSF.527-529.625
[17] K. Ohtomo, N. Matsumoto, K. Ashida, T. Kaneko, N. Ohtani, M. Katsuno, S. Sato, H. Tsuge, T. Fujimoto, Formation of basal plane stacking faults on the $(000\overline{1})$ facet of heavily nitrogen-doped 4H-SiC single crystals during physical vapor transport growth, J. Cryst. Growth 478 (2017) 174-179. https://doi.org/10.1016/j.jcrysgro.2017.09.008
[18] T. Ailihumaer, Y. Yang, J. Guo, B. Raghothamachar, M. Dudley, Studies on lattice strain variation due to nitrogen doping by synchrotron x-ray contour mapping technique in PVT-grown 4H-SiC crystals, J. Electron. Mater. 48 (2019) 3363-3369. https://doi.org/10.1007/s11664-019-07077-x
[19] N. Zhang, Y. Chen, E. Sanchez, D.R. Black, M. Dudley, The effect of 4H-SiC substrate surface scratches on chemical vapor deposition grown homo-epitaxial layer quality, Mater. Sci. Forum, 615 (2009) 109-112. https://doi.org/10.4028/www.scientific.net/MSF.615-617.109